Thermal wave pyroelectric thin film hydrogen sensor with extended detection dynamic range

Leonid M. Dorojkine*
Andreas Mandelis, MEMBER SPIE
University of Toronto
Photothermal and Optoelectronic Diagnostics Laboratories (PODL)
Center for Hydrogen and Electrochemical Studies
Toronto, Ontario M5S 3G8, Canada
E-mail: mandelis@me.utoronto.ca

Abstract. A novel thermal wave based pyroelectric thin film solid state sensor shown to be capable of responding to H_2 gas flows in N_2 or in air under ambient temperature and pressure conditions is described. The new sensor exhibits an extremely wide detection dynamic range: 100% to 25 ppm hydrogen in nitrogen, and a 10 to 90% signal rise time of approximately 10 s, limited by the inertia of the gas delivery system. The extended dynamic range is achieved through two complementary operating mechanisms, resulting in a thermophysical and a chemical response at high and low H_2 concentrations, respectively.

Subject terms: photoacoustic and photothermal science and engineering; hydrogen; sensor; thermal wave; pyroelectric; thermophysical; chemical.

Paper PPS-19 received May 1, 1996; revised manuscript received June 1, 1996; accepted for publication June 15, 1996.

1 Introduction

Recently, a concerted effort has been made to produce solid state hydrogen gas sensors using the photopyroelectric (PPE) effect, i.e. the production of an ac voltage (or current) across a pyroelectric element [usually polyvinylidene fluoride (PVDF)], resulting from photothermal excitation by an intensity-modulated laser beam.[1] The resulting PPE signal is caused by a thermal wave, the amplitude and phase of which are easily measured by a lock-in amplifier with the added benefit of a high SNR afforded by this narrow-band frequency demodulation scheme. Two operating modes have been identified for the PPE sensor. When the device is coated with a catalytic thin-film such as Pd, as an electrode, a mainly chemical response is observed on exposure to ambient hydrogen gas. The mechanism is consistent with a change in the optical reflectance of the Pd-coated surface on hydrogen adsorption and absorption,[2] possibly accompanied by a change in the pyroelectric coefficient of the active (PVDF) element.[3] When the device is coated with noncatalytic metal film electrodes (e.g., Al-Ni alloys), a purely thermophysical response is observed on exposure to hydrogen. This is consistent with a change in the boundary conditions (thermal coupling coefficients) of the PPE thermal wave field in the active element due to the increased thermal effusivity of hydrogen, which displaces other ambient gases[4,5] (nitrogen, air, etc.). The two operating modes coexist in Pd-coated devices and have been known to contribute in a complementary manner in different hydrogen gas concentration regimes.[2] They have been separated out by use of a reference sensor without a catalytic coating.[2] One of the drawbacks of PVDF PPE sensors is the low pyroelectric coefficient of the active element (3×10^{-9} C/cm^2 K, Ref. 6), which results in relatively low signal dynamic range compared to other pyroelectrics (e.g., $LiTaO_3$; Ref. 7).

In this paper, we exploited the improved pyroelectric performance of a thin film pyroelectric material, to fabricate a novel thermal wave solid state pyroelectric hydrogen sensor of extended dynamic range, by combination of its physical and chemical responses. To our knowledge, this new sensor exhibits one of the highest dynamic ranges for H_2 detection reported.[1] The pyroelectric element is an organic crystalline spatially oriented film, which differs substantially from its commonly used inorganic analogs CdS, ZnO, and AlN. Molecularly, it is a polycyclic organic compound (POC) and its molecules contain -NH_2 groups. The POC crystals belong to the noncentrosymmetric polar mm2 point group (a crystallographic classification that describes two distinct types of mirror planes containing a two-fold axis), and hence they possess both piezoelectricity and pyroelectricity. The film consists of spherolite blocks of typical dimensions 0.2 to 0.5 mm, each with its own orientation. In spite of the spatial inhomogeneity, the POC film exhibits very high pyroelectric and piezoelectric properties. It has been used for the pyroelectric detection of laser pulses and ''hot'' molecular beams[8,9] and as the active element in high-frequency wideband piezoelectric transducers.[10,11] The pyroelectric coefficient of POC is 5×10^{-9} C/cm^2 K.

2 Sensor Design and Fabrication

Based on the foregoing considerations, a number of thermal wave pyroelectric-film sensors (TWPFSs) were fabricated. Figure 1 shows a sideways cross section of a typical TWPFS design. The pyroelectric film was ~ 2 μm thick; the top electrode was an Al film, and the bottom electrode was made of Au (~ 0.3 μm) with a very thin Cr sublayer (a Cr-Au electrode). The morphology of the top electrode (thickness ≈ 0.15 μm) was not uniform but rather mesh-

*On leave from the Russian Academy of Sciences, N.S. Kurnakov Institute of General and Inorganic Chemistry, Moscow, Russia.

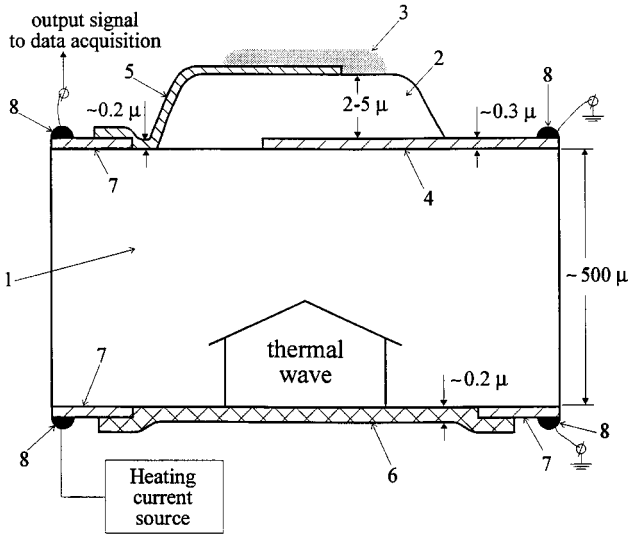

Fig. 1 Side-view cross section of the TWPFS design: 1, substrate (sitall, glass, ceramic, silica, sapphire, quartz; see text); 2, pyroelectric thin film; 3, chemically sensitive catalytic coating (Pd); 4, bottom electrode (Cr-Au or Cr-Ni); 5, top electrode (Al); 6, resistive heater Cr-Ni strip; 7 and 8, electrical contact pads (Cr-Au or Cr-Ni).

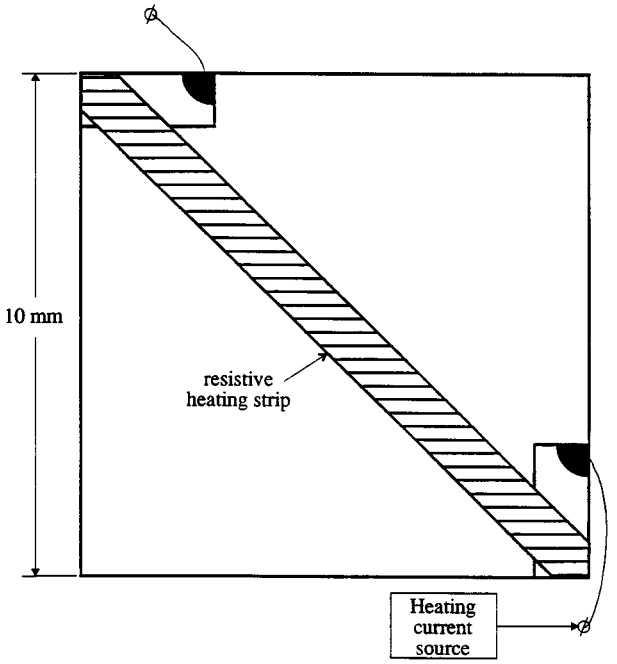

Fig. 3 Bottom view of the TWPFS design.

like, yielding a high specific surface area to facilitate the access of ambient gas molecules to the pyroelectric POC element. The top view of the sensor element is shown in Fig. 2; the active area, defined by the intersection between the top and bottom electrodes, was ~ 4.0 mm^2. As a thermally conductive substrate a ceramic (''sitall'') was used; it is based on SiO_2-Al_2O_3 and its thermal conductivity is $k = 0.015$ W/cm K. Conventionally, this ceramic is used as a heat sink in the Russian microelectronics industry. The substrate dimensions were $10 \times 10 \times 0.45$ mm^3. The capacitance of the pyroelectric POC element was in the range of 120 to 200 pF and its resistance was $\sim$ 0.5 to 2.0 GΩ. Unlike earlier PPE sensors, the TWPFS uses a resistive thermal source of short thermal time constant to generate thermal waves in the manner shown in Fig. 1. A resistive (50-Ω) strip of Cr-Ni alloy film was deposited diagonally across the bottom of the square substrate (Fig. 3), and its soldered edges were contacted to an ac voltage generator (KROHN-HITE Model 5100A). The same voltage source was used to supply the reference square-wave signal to the lock-in amplifier (EG&G PARC Model 5210). Some sensors were further coated with 300- to 500-Å Pd film deposited over the Al electrode to give the sensor catalytic properties with respect to H_2 gas,[12] i.e., chemical behavior.

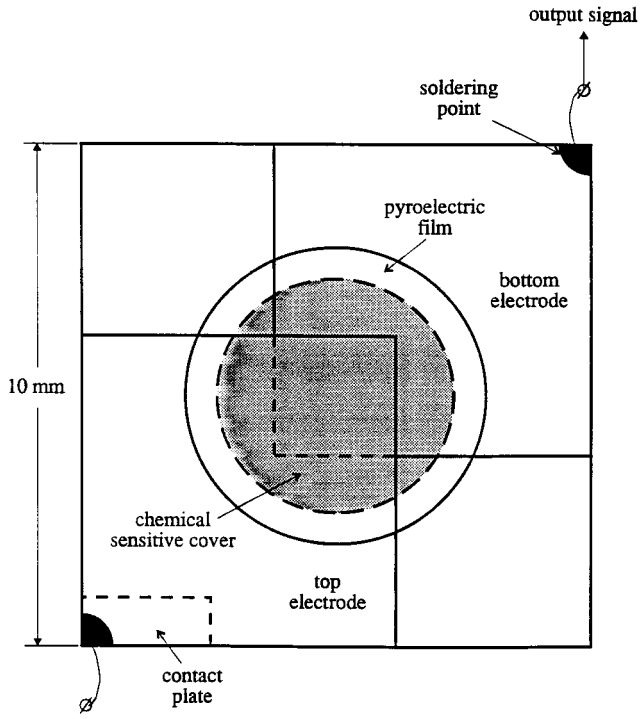

Fig. 2 Top view of the TWPFS design.

3 Experiment

The experimental set up is shown in Fig. 4. It consists of a gas cell, gas manifold, and delivery system; a thermal wave voltage generator; signal detection instrumentation; and data acquisition hardware and software. The gas cell was a small-volume ($\sim$40-cm^3) semicylinder designed so as to minimize the sensor response time to hydrogen flux into the cell. The cell included a semicylindrical glass cover with a metallic overlayer to shield against the overhead room lights and ambient electromagnetic interference, which tended to contribute to noise. All electrical input-output cables were coaxially grounded for the same reason. A TWPFS sensor could be mounted on the flat backing of the cell and securely positioned by four copper clamps. Two of these clamps were also used as electrical contacts for the delivery of the heating voltage to the resistive strip of Fig. 3; the other two were also used as conduits carrying the

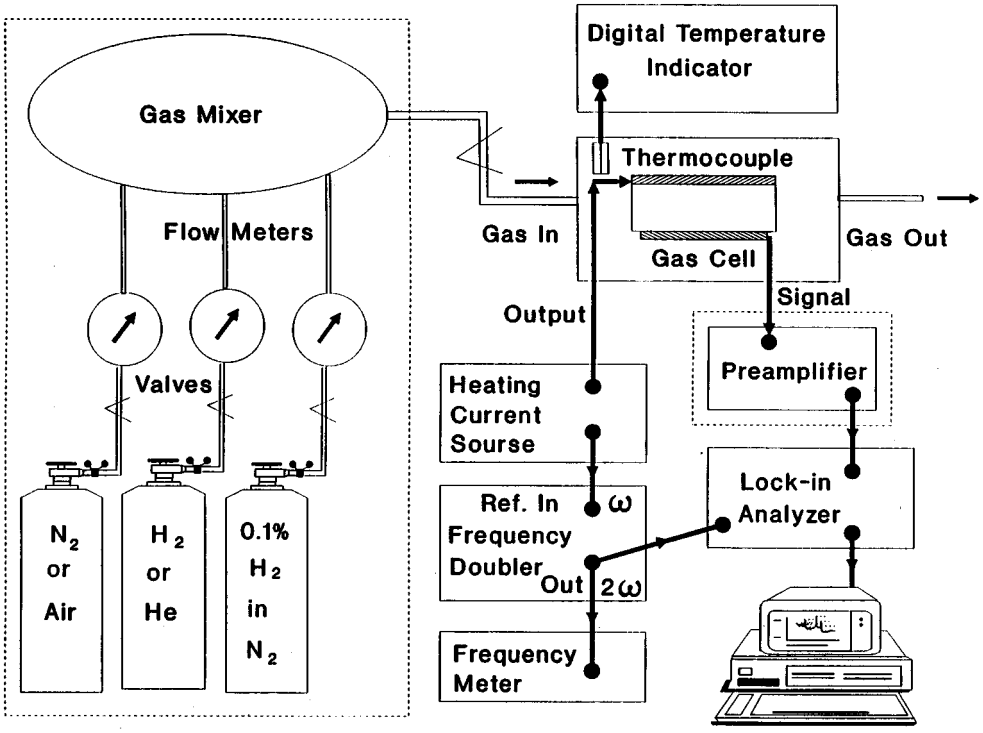

Fig. 4 Schematic of the experimental setup.

pyroelectric signal out of the cell and into the lock-in amplifier. Owing to the very good signal-to-noise ratio (SNR) throughout the subsequent experiments, it was found to be unnecessary to use a reference sensor simultaneously with the tests on the active sensor element. Any comparisons between different sensors were made after sequential testing.

The sine mode of the voltage generator signal was applied across the electrical contacts of the resistive heater. The range of signal voltage was 3- to 20-V peak-to-peak (p-t-p) amplitude and 4- to 15-Hz frequency. The optimal values for each experiment were chosen empirically. The 5-V p-t-p square-wave reference signal from the voltage generator was inserted in the lock-in reference channel. The harmonic voltage at $f = \omega/2\pi$ generates an ac current across the resistive element, which produces joule heating at $2f$ with thermal flux:

$$Q(2\omega,t)=\frac{1}{R}\,(V_0 \sin \omega t)^2=\left(\frac{V_0^2}{2R}\right)(1-\cos 2\omega t). \qquad (1)$$

Here R is the resistance of the metal strip and V_0 is the input voltage amplitude. Therefore, the lock-in signal could be monitored either at the second harmonic of the reference channel frequency using the $2f$ lock-in mode, or by use of a frequency doubler and first-harmonic detection. It was found that the latter method produced higher output signals in the 2- to 30-mV range, and thus it was adopted for most experiments, eliminating the need for a further preamplification stage, as shown in Fig. 4. A voltage amplifier (Ithaco Model 1201 low-noise preamplifier) was occasionally found useful for the detection of microvolt-level signals.

The gas delivery system (gas tanks, pressure/flow regulators, gas-flow meters, valves, and plastic connector tubing) included high-purity (99.999%) nitrogen, air, hydrogen, and helium gases, helium/nitrogen mixtures in the 0.2 to 100% range, as well as prepared mixtures of 1 and 0.1% hydrogen in nitrogen. The gases were purchased from Canadian Liquid Air Ltd. Gas mixtures of other H_2 concentrations were prepared in the laboratory by regulating the flow rates of the appropriate gases. Two types of flow meters were used: a high-precision 1 to 11 ml/min gauge and high-flow 60 to 500 ml/min gauges. Through proper interconnections of gas tanks and flow meters, the gas delivery system was capable of supplying hydrogen/nitrogen mixtures in the range between 100% and 10 ppm, and helium/nitrogen mixtures in the range $\geqslant 0.2\%$. The total gas flow was kept at the level of 300 to 500 ml/min. The full gas transport length between tanks and gas cell was $\sim$2.5 m so as to attain reliable ambient temperature control of the gas flow with no need for external heat exchangers, as verified by the gas-cell thermocouple readout. The price paid for ensuring temperature stability was that the tubing length became the limiting factor in the cell response to gas flow, by adding an excess volume estimated to be $\sim$60 cm^3. As a result, the effective sensor rise time was measured to be 15 to 20 s for all our experiments, but the actual device rise time with Pd coating was monitored using a Boonton Model 7200 Capacitance Meter and under conditions identical to those used for the pyroelectric signal acquisition. The quality of capacitance signals was much poorer than that of the pyroelectric responses.

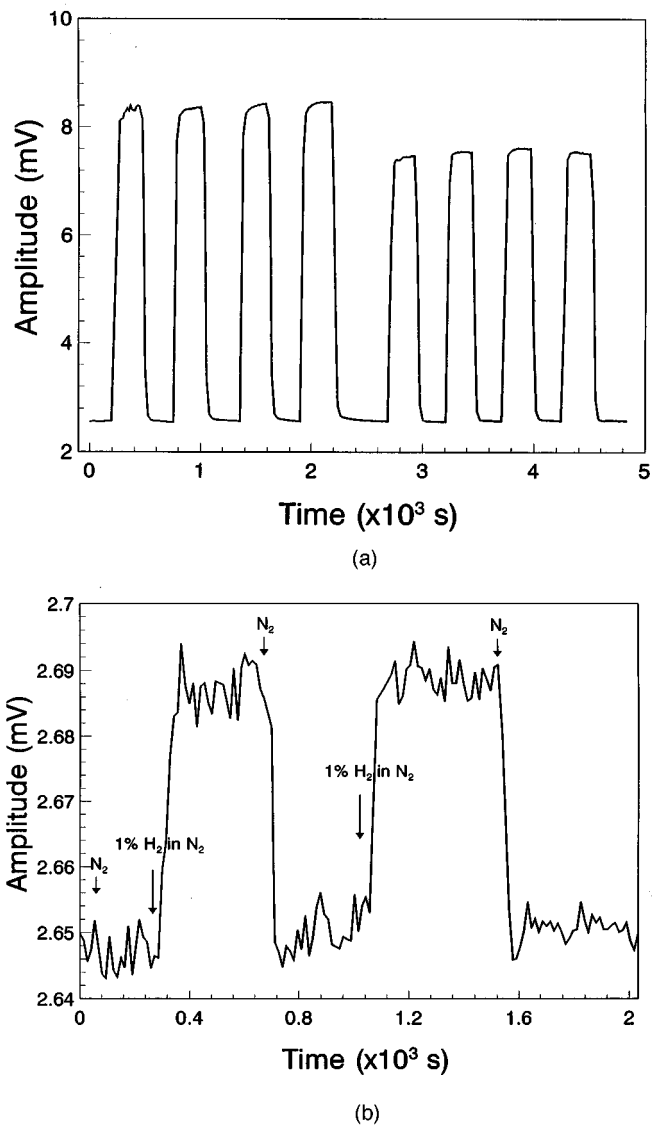

Fig. 5 Time profiles of the thermophysical amplitude response of the TWPFS: (a) 100% H_2 (left half) and He (right half) in nitrogen background gas and (b) 1% H_2 in N_2. Gas flow-rates, 500 ml/min; ambient temperature $T=22$ °C; heating source voltage $V=10$ V p-t-p at $f=4$ Hz.

4 Results

4.1 *Thermophysical Response*

The thermophysical response was studied using POC active element sensors without Pd coating. Selected response-time profiles of the TWPFS are shown in Fig. 5. Both amplitude and phase channels were monitored and they usually exhibited similar quality and SNRs. Nevertheless, for the sake of conciseness, mostly amplitude data are presented. Figure 5(a) shows repetitive time profiles of the sensor response to 100% hydrogen and 100% helium. Relative normalized lock-in voltage amplitudes at saturation are plotted in that figure:

$$S([G])=\frac{V([G])-V([N_2])}{V([N_2])}, \tag{2}$$

where G stands for either H_2 or He. As expected,[5] the He response is somewhat smaller than the H_2 response due to the fact that the thermal effusivity of He is closer to that of the background gas (nitrogen) than that of H_2. The reproducibility of the sensor data, its reversibility, and signal quality are as good as, or better than, the earlier data obtained from the PVDF-based hydrogen sensor,[5] whereas the signal strength is much better than the PVDF device because of the higher pyroelectric coefficient and the much larger effective surface area. Figure 5(b) shows the response to 1% H_2 exhibiting an SNR of approx. 7–8 which assures adequate detectivity in the 0.1% range. Similar quality responses to 1% He gas in nitrogen were also obtained. The SNR of the PVDF sensor response to 1% hydrogen in air was ~ 3 to 4. The TWPFS responses are symmetric with respect to the gas on/off transients, which is indicative of a single mechanism of operation. A thermal wave model of the PVDF-based sensor was presented earlier[5] and fitted to the H_2 and He ambient data, thus verifying the thermophysical origin of the observed signals and the absence of any chemical interaction between the sensor and the ambient gas. A major difference between the amplitude responses of the PVDF-based and the present POC-based sensors is the opposite direction of the signal changes: on the introduction of hydrogen gas in the cell the PVDF-based sensor's amplitude decreased,[4] whereas the POC-sensor's amplitude increased (Fig. 5). The former behavior can be explained based on the fact that hydrogen is a better thermally conducting medium than the displaced air (or nitrogen), inducing a larger thermal loss across the sensor-gas interface boundary, which decreases the thermal wave signal.[5] In this case, the pyroelectric signal depends on the thermal power content of the relatively thick (~ 28 to 52 μm) sensor bulk averaged over its thickness, and the pyroelectric layer acts as a pyroelectric calorimeter.[13] For the POC sensor, no detailed thermal wave model has been developed; nevertheless, the amplitude increase is expected to be partly the result of the increased temperature gradient between the front (top) and back (bottom) surfaces of the pyroelectric thin film due to the cooling of the top surface of the film (Fig. 1), on exposure to ambient hydrogen gas. The pyroelectric signal from this relatively thin (~ 2 μm) layer is proportional to the thickness-averaged temperature difference between top and bottom planes, and the POC element acts as a pyroelectric thermometer.[13] Furthermore, another amplitude increase mechanism is expected to operate and even dominate the signal under certain conditions: the thermal wave field distribution in the cell is complicated by the presence of several planar surfaces acting as thermal wave reflection interfaces and by gas strips, which are, in principle, capable of sustaining signal enhancing standing thermal wave patterns (resonances). Therefore, signal ''tuning'' and optimization by sweeping the frequency or by changing the ambient gas can be expected and has, indeed, been observed in the course of our experiments. Capacitance measurements using the nonpalladianized POC sensor failed to show any response above the noise floor, thus providing further proof of the totally thermophysical nature of the thermal wave pyroelectric signals described in Fig. 5.

The base line of all reported pyroelectric experiments remained essentially constant over periods of several hours.

Any signal drift was traced to the thermalization of the detection electronics and was almost eliminated by keeping all the electrical components turned on even during prolonged periods when no experiments were being performed. The signal-amplitude saturation level S dependence [Eq. (2)], on hydrogen concentration is shown in Fig. 6. On the same figure the response to He gas is given for comparison purposes and as proof of the thermophysical origin of the signals. Figure 6(a) shows coarse-interval results obtained with the high-flow gauge in the 4 to 100% range and exhibits a distinctly nonlinear behavior of the isotherm. Figure 6(b) covers the 0.5 to 4% range, in which both the $S([H_2])$ and $S([He])$ responses on the concentration of these gases in nitrogen are linear.

The rise time of the TWPFS to a 100% hydrogen ''pulse'' in nitrogen is shown in Fig. 7. The observed 0 to 90% of the saturation value rise time was ~ 15 s. This delay was mostly attributed to the inertia of the gas delivery system. Finally, only a slight dependence of the pyroelectric signals on gas flow rate was observed: for flow rate changes in the 100 to 500 ml/min range, the sensor signal saturation value varied by up to 8%.

4.2 *Chemical Response*

For these measurements a Pd-coated POC sensor was used and both H_2 and He gas flows were tested in nitrogen carrier gas. It was found that the chemical sensor responds to the presence of He down to $\sim 0.15\%$. The sensitivity of its response to hydrogen was much higher and opposite in sign to that of He, as shown in Fig. 8. The response to He is thermophysical, with the pyroelectric signal amplitude increasing on exposure to that gas, as expected from the foregoing results in Sec. 4.1; on the other hand, the amplitude decreased on introduction of hydrogen gas in the $<0.1\%$ concentration range. Furthermore, the chemical response always exhibited asymmetric behavior with respect to hydrogen on/off thresholds. The sign and symmetry differences in the responses shown in Fig. 8 make the identification of the signal origin quite easy, an important feature of the TWPFS. Quantitatively, the sensor recovery time in the chemical mode was measured to be of the order of 1/2 h, as compared to a few minutes for the rise time (and a few seconds for the thermophysical response rise time, Fig. 7). Figure 9 shows the highest sensitivity of the chemical TWPFS device so far achieved through its response to 25 ppm of H_2 in N_2. The SNR is 5 to 6 and indicates an extrapolated potential for detecting 4 to 5 ppm in a single-ended mode (i.e., without a reference sensor). The current lowest level of 25 ppm is well below the prior level of 40 ppm obtained using the photopyroelectric Pd-PVDF sensor.[14] The detectivity limit here was set by the capabilities of the gas delivery system and the gas mixtures available. A further improvement may be possible by using a reference sensor in the common rejection mode configuration.

Figure 10 is the isotherm for the chemical response of the Pd-coated TWPFS and exhibits essential linearity between 25 and 1000 ppm, except for the lowest concentrations/signals in which noise interferes with the linearity of the response. No response from He could be obtained in this entire range, with the exception of a small (positive amplitude S) thermophysical signal in the uppermost range $\geqslant 1000$ ppm. In Fig. 10, only data on hydrogen concentrations below 1000 ppm are presented, because this regime is optimal for chemical sensing and thus complementary to the isotherms of Fig. 6. Nevertheless, the threshold concentration of H_2 gas for chemical sensing was in the 1200- to 1500-ppm range. Together, the three H_2-Pd isotherms in Figs. 6(a), 6(b) and 10 span 25 ppm to 100% H_2 in nitrogen, almost five orders of magnitude in complementary thermophysical-chemical sensitivity. Attempts to use the chemical Pd-TWPFS to monitor hydrogen concentrations >1200 to 1500 ppm were proven to yield results inferior to the thermophysical nonpalladianized TWPFS: the signals were characterized by spurious jumps accompanied by random sign changes and extraordinarily long recovery times (>1 h). Although both mechanisms are present in the Pd-TWPFS, these facts accentuate the essential complementarity of the thermophysical and chemical POC sensors, as well as their absolute compatibility, as manifested by the continuous and smooth passage at $\sim 0.1\%$ H_2 in N_2 from the physical to the chemical operating mechanism, across the very wide combined dynamic detection range.

Capacitance measurements were made under conditions identical to those of Figs. 8 to 10. The results are shown in Fig. 11 for 1000 ppm H_2 in N_2 reference gas. The signal levels were quite low with SNR ~ 4 to 5 for 1000 ppm H_2 and further worsening down to ~ 1.0 to 1.3 for 500 ppm H_2 in nitrogen, the absolute minimum detection level using capacitive sensing. Another problem faced by the present computer-aided detection set up in Fig. 11 is the limitations imposed by the 12-bit analog-to-digital (A/D) converter. Nevertheless, it can be discerned that the upward and downward transients of Fig. 11 exhibit asymmetric time constants, with the decay times being longer than the rise times, a feature similar to the pyroelectric chemical responses of Fig. 8. On exposure of the Pd-TWPFS to 100% He, no net increase of the capacitive signal was observed in Fig. 11, as expected. There seems to be a noise-level disturbance resulting from the introduction of He in the gas cell, however, the level is entirely within the background noise floor. No photochemical or photoelectric responses of the sensor were likely, since the signal detection always occurred in the dark under the cover of the metallic layer of the gas cell. Experiments with the intensity-modulated beam of an Ar-ion laser showed a very strong PPE response of the POC sensor under photothermal excitation, but these results are outside the scope of the present investigation.

5 Discussion

From the microscopic (molecular) point of view, the probable mechanism of the hydrogen chemical effect on the Pd-Al-POC active element of the TWPFS lies with the catalytic properties of the Pd layer[15] in the process of the dissociation of the hydrogen molecule:

$$H_2 \overset{Pd}{\rightleftarrows} 2H. \tag{3}$$

Following dissociation and diffusion through the porous Pd-Al layer, monoatomic hydrogen atoms reach the POC film, which is in intimate molecular contact with the over-

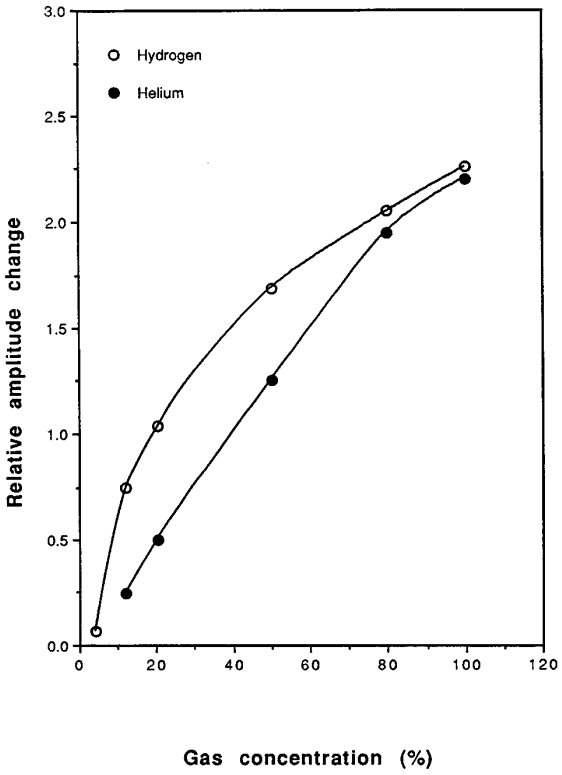

(a)

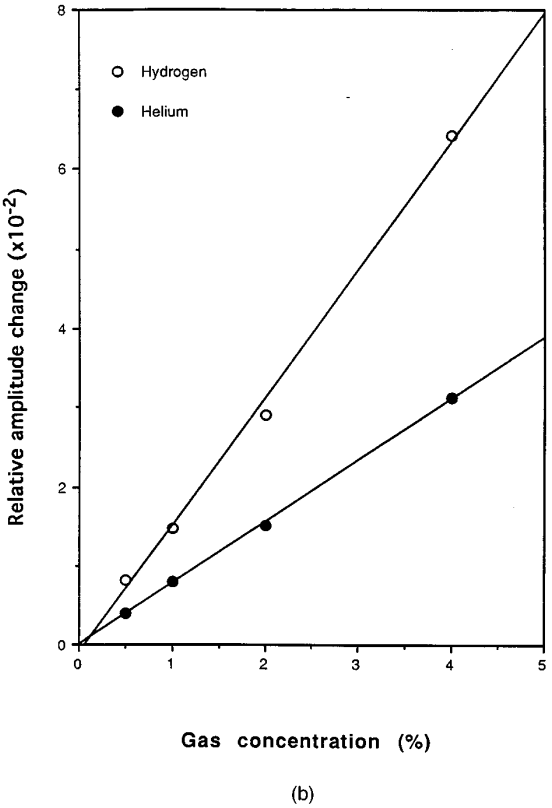

(b)

Fig. 6 Isotherms of the TWPFS thermophysical response to H_2 and He gases in ambient N_2 gas: (a) coarse concentration range 4 to 100% and (b) fine concentration range 0.5 to 5%. Sensor instrumentation and ambient parameters are as in Fig. 5.

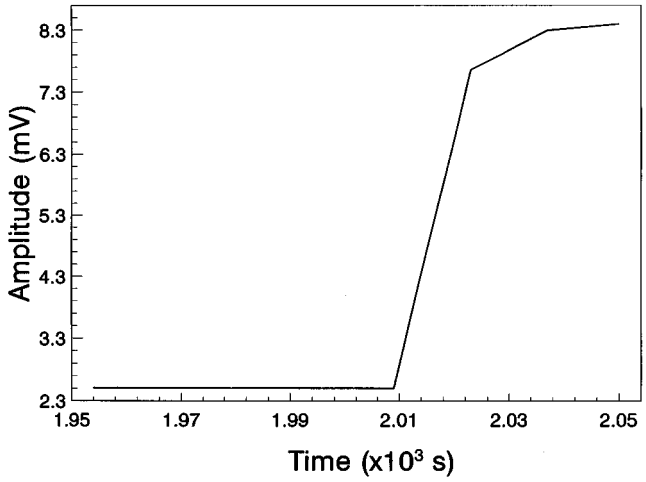

Fig. 7 Rise time of the TWPFS thermophysical response to H_2 gas in ambient N_2 gas.

layer. The following reversible chemical reaction between atomic hydrogen and the $-NH_2$ groups of the POC layer is likely:

$$-NH_2 + H \rightleftarrows -NH_3 . \tag{4}$$

This reaction results in the change of both the molecular configuration and the crystallinity of the POC structure.[16] Therefore, reversible changes of the individual microcrystal properties and the character of their spatial orientation are expected. The most probable outcome of this reconfiguration is the reduction of the pyroelectric coefficient of the Pd-coated POC. This is in qualitative agreement with the experimental data, which exhibit decreased, reversible thermal wave amplitudes on exposure to hydrogen gas.

From the macroscopic viewpoint, the amplitude of the pyroelectric response depends on the values of the pyroelectric coefficient and the dielectric constant (i.e., the ca-

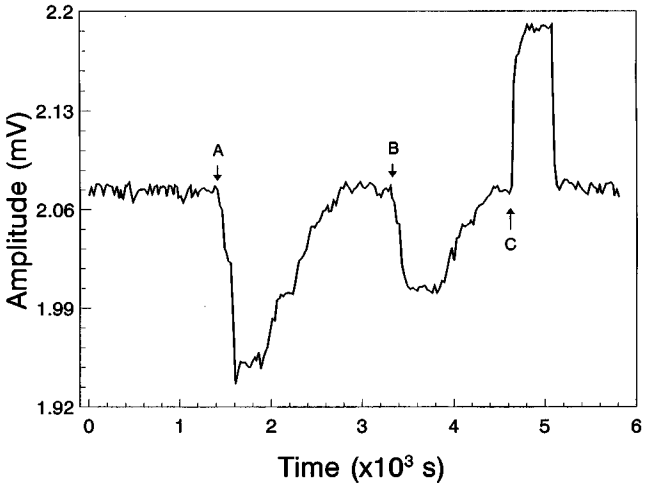

Fig. 8 Pd-TWPFS amplitude profiles on exposure to *A*, 1000 ppm H_2; *B*, 500 ppm H_2; and *C*, 15% He. Responses *A* and *B* are chemical; response *C* is thermophysical. The arrows indicate the onset of gas introduction. N_2 was the background gas in all cases.

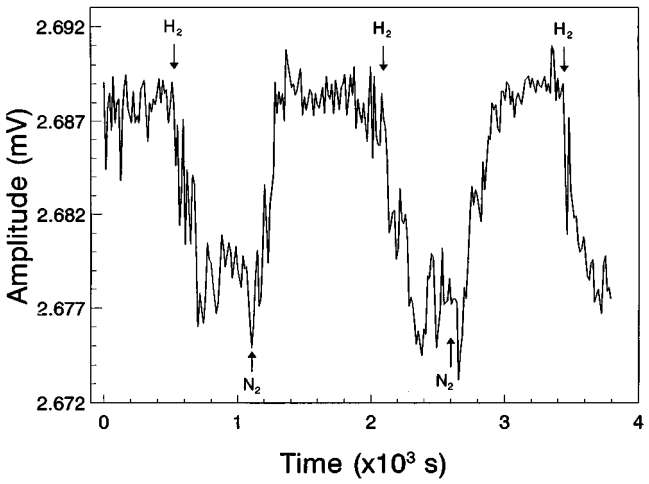

Fig. 9 Pd-TWPFS chemical response to 25 ppm hydrogen gas in nitrogen. The arrows indicate the onset of gas introduction.

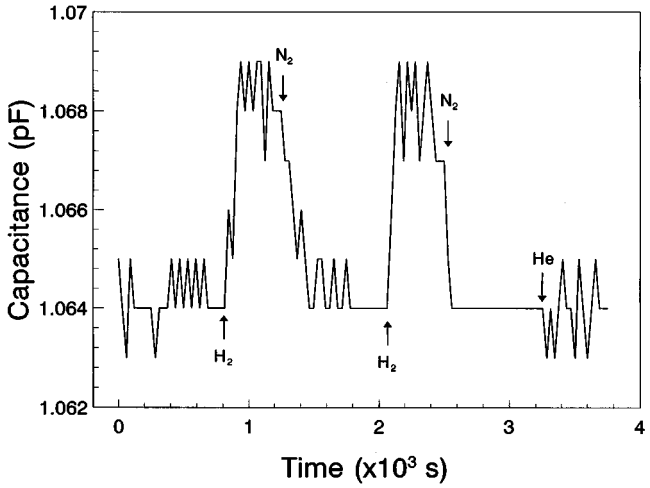

Fig. 11 Pd-TWPFS capacitance response to 1000 ppm H_2 and to 100% He, both in nitrogen gas background. The arrows indicate the onset of gas introduction.

pacitance) C_p of the POC films. The capacitance measurements of Fig. 11, made under hydrogen and helium exposures, showed no response to the latter gas. Similar exposures to atmospheres of synthetic air and nitrogen showed no change in capacitance either. On exposure to 1000 ppm H_2, however, a change in the capacitance ΔC_p of the pyroelectric by $\sim 0.5\%$ was observed, while 100% He showed no observable C_p change. For exposure to 500 ppm H_2, a relative capacitance change by $\sim 0.3\%$ was found, scaling linearly with that of Fig. 11. It is well known that the spontaneous polarization, that is, the excess charge, of a pyroelectric element in the presence of a temperature gradient ΔT is given by[17]

$$\Delta P = p \Delta T, \tag{5}$$

where p is the pyroelectric coefficient and is essentially independent of temperature. Only temperature changes can induce pyroelectric signals. The time-dependent pyroelectric excess charge generates an output pyroelectric current:

$$I_p = \frac{\mathrm{d}(\Delta P)}{\mathrm{d}t} = p \frac{\mathrm{d}(\Delta T)}{\mathrm{d}t}. \tag{6}$$

This current is proportional to the rate of change of the temperature. The output signal is usually the pyroelectric voltage V_p. This value depends on several electrical factors, as shown in Fig. 12. Among the many factors, the instrumental ones remain constant on exposure to different gaseous atmospheres, whereas the pyroelectric capacitance,

$$C_p = \frac{A_p \epsilon}{4\pi h}, \tag{7}$$

is affected by the dependence of the dielectric constant ϵ, and perhaps the pyroelectric thickness h on the chemical interaction between the gas and the pyroelectric element. Here A_p is the active pyroelectric area. The output pyroelectric voltage can be obtained by considering the equivalent circuit of Fig. 12:

$$V_p = p \frac{\mathrm{d}(\Delta T)}{\mathrm{d}t} \frac{R_i}{1 + 2i\omega\tau}, \tag{8}$$

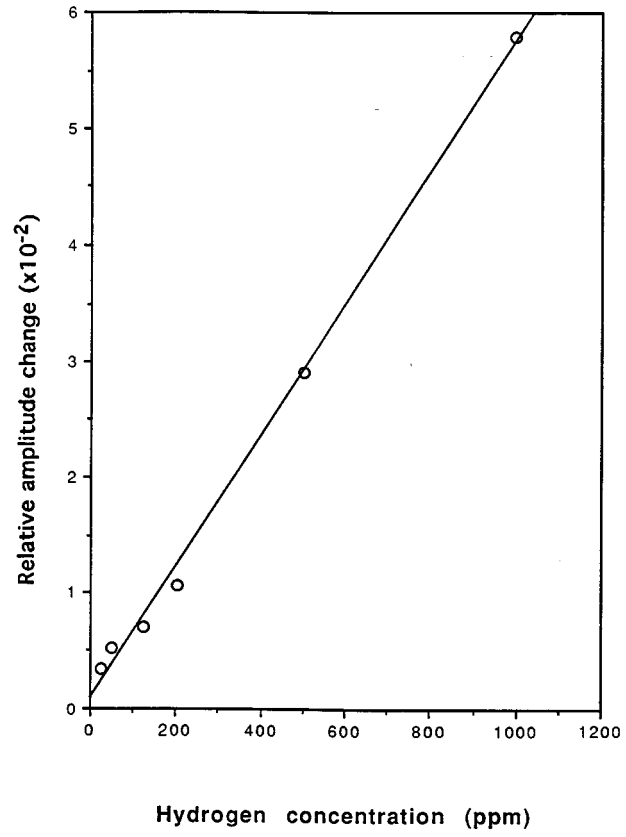

Fig. 10 Isotherms of the Pd-TWPFS chemical response to H_2 in ambient N_2 gas in the range 25 to 1000 ppm. Sensor instrumentation parameters are as in Fig. 5, and temperature is 22°C.

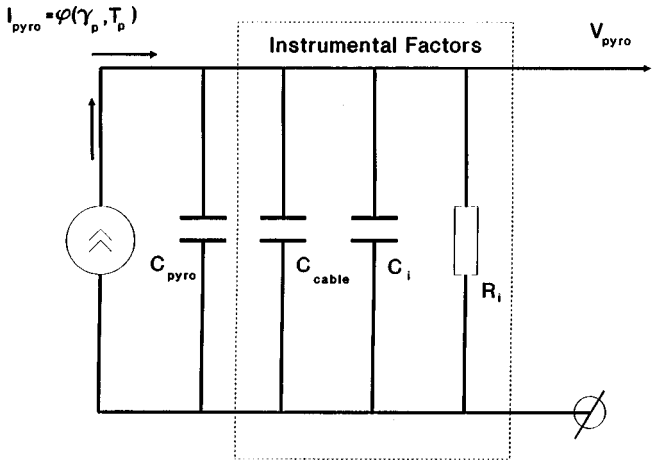

Fig. 12 Equivalent electrical circuit of the pyroelectric output voltage, as a function of system parameters. Here R_i and C_i are the input resistance and capacitance of the preamplifier connected to the pyroelectric circuit.

where R_i was defined in Fig. 12, and τ is the resistance-capacitance (R-C) time constant of the pyroelectric-preamplifier circuit in that figure:

$$\tau = R_i(C_p + C_{\text{cable}} + C_i). \tag{9}$$

Note that, according to Okuyama et al.,[18] the electrical signal equivalent circuit of the pyroelectric should include a source due to the difference in the work functions between the top and bottom metal electrodes of the electrical insulator (chemically active pyroelectric element). In the present work, several tests were performed with electrodes of different work functions (Al-Au, Al-Cr, Al-Ni, and the ''zero'' couple Al-Al), but no measurable effect on the pyroelectric thermal wave signal was observed.

In evaluating the effects of any change of C_p with hydrogen concentration on the output pyroelectric voltage, $\partial V_p / \partial C_p$ was calculated using Eqs. (8) and (9), and the fractional change ΔF was calculated from the pyroelectric voltage amplitude:

$$\Delta F[\mathrm{H_2}] = \frac{\partial V_p / \partial C_p}{V_p} \, C_p . \tag{10}$$

Substituting the experimental values in Eq. (10), the following results were obtained: $\Delta F[1000\ \text{ppm}] = 0.004$; $\Delta F[500\ \text{ppm}] = 0.002$. These values are of the same order of magnitude as the experimental values ($\sim 0.5\%$) obtained in Fig. 11. Therefore, it seems plausible to conclude that the major mechanism for the TWPFS chemical response to H_2 exposure is the change in the value of the dielectric constant $\epsilon[\mathrm{H_2}]$, which, in turn, possibly implies a change in the value of the pyroelectric coefficient $p = p[\mathrm{H_2}]$ through its dependence on ϵ. This would be consistent with the pyroelectric coefficient's definition as a measure of spatial order in the bulk of the pyroelectric material,[19] which is thus expected to be susceptible to small perturbations in the molecular and crystalline structure. The foregoing hypothesis was further supported by experiments using a test sensor with the geometry of Fig. 1, including a Pd layer but with an unpoled phenolphthalein film instead of POC material. High-quality 2-μm thick films of centrosymmetric phenolphthalein ($C_{20}H_{14}O_4$) were prepared by vacuum evaporation especially for this test. No measurable pyroelectric signal change was observable under any hydrogen exposure conditions, confirming the central role of pyroelectric transduction mechanism(s) in the operation of the TWPFS device. Conversely, capacitance measurements were made using a sensor with pyroelectrically active POC layer, but without Pd coating. No measurable signals could be observed under atmospheres of 100% or 1000 ppm hydrogen in nitrogen. Therefore, it must be concluded that the change in the Pd-TWPFS capacitance shown in Fig. 11 is most likely due to the chemical interaction between trapped hydrogen in a monatomic form and the molecules of the POC layer. Unfortunately, at this stage, the details of the dependence of either the pyroelectric coefficient, or the dielectric constant on the molecular composition and structure of POC are unknown. Information from separate thermal wave pyroelectric and capacitance measurements may not give unique answers to this question, because such measurements do not directly probe the $p[\mathrm{H_2}]$ and $\epsilon[\mathrm{H_2}]$ interdependence. The complex, nonideal crystallinelike structure of the POC in terms of spatially oriented crystalline domains further complicates the analysis.

6 Conclusions

A novel thermal wave pyroelectric hydrogen sensor has been fabricated and tested. The sensor was based on a POC with high pyroelectric coefficient. Thermal waves were launched using resistive heating of the sensor substrate ceramic. At high hydrogen gas concentrations ($>0.1\%$) in nitrogen, a thermophysical operation mode was dominant. In this concentration range, a noncatalytic Al-POC active element was found to give optimal thermal wave pyroelectric signals (both amplitude and phase). At low hydrogen concentrations ($<0.1\%$) in nitrogen, the exclusive mode of sensor operation was chemical. The combined dynamic range of the sensor currently spans 25 ppm to 100%. The thermophysical mechanism of the device operation was found to be consistent with simple thermometric action of the pyroelectric element. The chemical mechanism was found to be more complicated, most likely involving changes in the dielectric constant and the pyroelectric coefficient of the Pd-Al-POC structure. Capacitance measurements of the Pd-coated sensor exhibited much diminished sensitivity to hydrogen ambients, compared to the thermal wave pyroelectric signal transduction; nevertheless, these measurements highlighted the beneficial role of the dielectric constant on the transduction mechanism.

Acknowledgments

We are grateful to the Natural Sciences and Engineering Research Council of Canada for an International Scientific Award to one of us (L.D.), and to Natural Resources Canada for support that made this work possible.

References

1. A. Mandelis and C. Christofides, ''Physics, chemistry and technology of solid state gas sensor devices,'' Chap. 8, *Chemical Analysis* Vol.

125, J. D. Winefordner, Ed., Wiley, New York (1993).
2. R. Wagner and A. Mandelis, ''Separation of thermal-wave and optical reflectance effects in a palladium-photopyroelectric hydrogen sensor,'' *Ferroelectrics* **165**, 193–203 (1995).
3. A. Mandelis and C. Christofides, ''Photothermal electrostatics of the Pd-polyvinylidene fluoride photopyroelectric hydrogen gas sensor,'' *J. Appl. Phys.* **70**, 4496–4504 (1991).
4. M. Munidasa and A. Mandelis, ''Purely thermal wave based nonchemical photopyroelectric gas sensor: application to hydrogen,'' *Rev. Sci. Instrum.* **65**, 1978–1982 (1994).
5. M. Munidasa, A. Mandelis, A. Katz, D. V. Do, and V. K. Luong, ''Characterization of a purely thermal wave based photopyroelectric gas sensor for hydrogen detection,'' *Rev. Sci. Instrum.* **65**, 1983–1987 (1994).
6. *KYNAR Piezo Film Technical Manual*, Pennwalt Corp., King of Prussia, PA (1983).
7. J. N. Zemel, ''Microfabricated nonoptical chemical sensors,'' *Rev. Sci. Instrum.* **61**, 1579–1606 (1990).
8. L. M. Dorozhkin (variant of Dorojkine), V. V. Lazarev, G. M. Pleshkov, B. A. Chayanov, S. S. Nabiev, S. M. Nikiforov, E. M. Khokhlov, V. A. Chikov, V. D. Shigorin, and G. P. Shipulo, ''A thin-film piezoelectric receiver utilizing organic compounds for the measurement of laser radiation parameters,'' *Sov. J. Quantum Electron.* **10**, 1107–1113 (1983).
9. V. M. Apatin, L. M. Dorozhkin (variant of Dorojkine), G. N. Makarov, and G. M. Pleshkov, ''Diagnostics of pulsed molecular beams and free jets with pyroelectric detectors and TEA CO_2 lasers,'' *Appl. Phys. B* **29**, 273–278 (1982).
10. A. I. Morozov, M. A. Kulakov, L. M. Dorozhkin (variant of Dorojkine), G. M. Pleshkov, and B. A. Chayanov, ''Organic piezoelectric thin-film transducers,'' *Electron. Lett.* **18**, 878–879 (1982).
11. I. A. Veselovsky, L. M. Dorozhkin (variant of Dorojkine), V. V. Lazarev, V. G. Mikchalevich, G. M. Pleshkov, A. M. Rodin, and B. A. Chayanov, ''A piezoelectric transducer, based on organic polycrystalline film for measurements of pulse characteristics,'' *Sov. Phys. Acoust.* **33**, 834–838 (1987).
12. F. A. Lewis, *The Palladium-Hydrogen System*, Academic, New York (1967).
13. H. Coufal and A. Mandelis, ''Photopyroelectric spectroscopy of semiconductors,'' Chap. 7 in *Photoacoustic and Thermal Wave Phenomena in Semiconductors*, A. Mandelis, Ed., pp. 149–173, North-Holland, New York (1987).
14. C. Christofides and A. Mandelis, ''Operating characteristics and comparison of photopyroelectric and piezoelectric sensors for trace hydrogen gas detection. Part I: development of a new photopyroelectric sensor,'' *J. Appl. Phys.* **66**, 3975–3985 (1989).
15. I. Lundstrom, ''Hydrogen sensitive MOS-structures. Part 1: principles and applications,'' *Sens. Actuat.* **1**, 403–426 (1981).
16. A. I. Kitaigorodsky, *Molecular Crystals and Molecules*, Academic, New York (1973).
17. J. F. Nye, *Physical Properties of Crystals*, pp. 78, 189, Oxford University Press, Oxford (1957).
18. K. Okuyama, N. Takinami, Y. Chiba, S. Ohshima, and S. Kambe, ''Al-Al_2O_3-Pd junction hydrogen sensor,'' *J. Appl. Phys.* **76**, 231–235 (1994).
19. M. G. Broadhurst and G. T. Davis, in *Electrets*, pp. 285–319, Springer-Verlag Topics in Applied Physics, Vol. 33, Springer-Verlag, Berlin (1987).

Leonid M. Dorojkine received his degree in physics and his PhD in physics from Moscow College of Physics and Technology in 1973 and 1977, respectively. From 1977 to 1991 he worked on crystalline material development for lasers and nonlinear optics, thin film piezoelectric and pyroelectric materials at the Institute of General Physics and the Institute of Intermediates and Dyes. In 1991, he joined the N.S. Kurnakov Institute of General and Inorganic Chemistry where he is currently researching chemical sensors. Dr. Dorojkine is a laureate of the highly prestigious Leninsky Comsomol Prize Laureate (1983). In 1994, he received an award of the National Science and Engineering Research Council of Canada. His research interests include nonsymmetrical crystalline materials and applications, chemical sensors, optoacoustics, and thermosphysical phenomena.

Andreas Mandelis: Biography and photograph appear with the special section guest editorial in this issue.